

# Discrete knot ejection from the jet in a nearby low-luminosity active galactic nucleus, M81\*

Ashley L. King<sup>1\*</sup>, Jon M. Miller<sup>2</sup>, Michael Bietenholz<sup>3,4</sup>, Kayhan Gültekin<sup>2</sup>, Mark T. Reynolds<sup>2</sup>, Amy Mioduszewski<sup>5</sup>, Michael Rupen<sup>6</sup> and Norbert Bartel<sup>3</sup>

**Observational constraints of the relativistic jets from black holes have largely come from the most powerful and extended jets<sup>1,2</sup>, leaving the nature of the low-luminosity jets a mystery<sup>3</sup>. M81\* is one of the nearest low-luminosity jets and it emitted an extremely large radio flare in 2011, allowing us to study compact core emission with unprecedented sensitivity and linear resolution. Using a multiwavelength campaign, we were able to track the flare as it re-brightened and became optically thick. Simultaneous X-ray observations indicated that the radio re-brightening was preceded by a low-energy X-ray flare at least 12 days earlier. Associating the time delay ( $t_{\text{delay}}$ ) between the two bands with the cooling time in a synchrotron flare<sup>4,5</sup>, we find that the magnetic field strength was  $1.9 < B < 9.2$  G, which is consistent with magnetic field estimate from spectral energy distribution modelling<sup>6</sup>,  $B < 10.2$  G. In addition, Very Long Baseline Array observations at 23 GHz clearly illustrate a discrete knot moving at a low relativistic speed of  $v_{\text{app}}/c = 0.51 \pm 0.17$  associated with the initial radio flare. The observations indicate radial jet motions for the first time in M81\*. This has profound implications for jet production, as it means radial motion can be observed in even the lowest-luminosity AGN, but at slower velocities and smaller radial extents ( $\approx 10^4 R_g$ ).**

M81\*, at a distance of  $3.96 \pm 0.29$  Mpc (ref. 7), is one of the nearest low-luminosity active galactic nuclei (AGN), and has a black hole mass of  $7^{+2}_{-1} \times 10^7 M_\odot$  (ref. 8). It has been well surveyed at many frequencies, including the radio<sup>9–12</sup> and X-ray<sup>13–15</sup> bands. Like many other low-luminosity AGN, the X-ray and radio luminosities of M81\*, along with its mass, place it on the ‘fundamental plane of black hole activity’<sup>3,14</sup>. The existence of this plane suggests a functional relationship between the jet production level, as indicated by the 5 GHz radio luminosity, the 2–10 keV X-ray emission and the black hole mass<sup>3,14</sup>.

Although M81\* fits on the fundamental plane within small fluctuations around its mean<sup>16</sup>, it shows highly variable radio emission<sup>17</sup> at frequencies greater than 5 GHz. At 15 GHz, M81\* has an average flux density of 116 mJy (ref. 18) with typical flares reaching on the order of 150 mJy (ref. 17). In 2011 M81\* exceeded its typical flare strength, increasing from a flux density of 140 mJy on 24 August 2011 (modified Julian date (MJD) 55797), to 261 mJy and 321 mJy on 27 August 2011 (MJD 55800) and 1 September 2011 (MJD 55805), respectively<sup>18</sup>. Observers assembled a campaign in both the radio and X-ray bands to track this substantial brightening, never before observed in a low-luminosity AGN of such proximity.

We targeted M81\* with four epochs of radio observations, including both broadband frequency coverage with the K. Jansky Very Large Array (VLA) and high-resolution radio imaging with the Very Long Baseline Array (VLBA). Figure 1a,b illustrates the VLA broadband radio frequency behaviour in the unresolved compact core. As indicated by the decrease in flux density between 17 September and 21 September, the flare was already cooling nearly 20 days after the initial report of activity. The radio spectral index,  $\alpha$  (where  $S_\nu \propto \nu^\alpha$ ;  $S_\nu$  is the flux density and  $\nu$  is the frequency), was negative, consistent with optically thin synchrotron emission. However, by the end of the four epochs the radio emission at higher frequencies had re-brightened and the spectral index was consistent with optically thick synchrotron emission ( $\alpha > 0$ ). This indicates renewed flaring activity at very small radii, that is, at the core of the jet. VLBA observations confirm this, and will be discussed below.

Compact radio core emission is generally modelled as self-absorbed synchrotron emission<sup>19</sup>. The peak in the spectrum occurs at the boundary between the optically thick and optically thin emission, from which we can make an estimate of  $B$  (ref. 6). Our first epoch observations peak at  $\nu_{\text{peak},1} = 10.4^{+1.0}_{-2.5}$  GHz with a flux density of  $S_p = 0.22 \pm 0.01$  Jy. Taking the restoring beam from the 8.4 GHz VLBA observations as an upper limit to the size of the core, we find  $B \lesssim 10.2$  G. See Supplementary Information for more details. During the second epoch, the second flare peaks at roughly  $\nu_p \sim 28$  GHz, but with only a few data points at higher frequencies it is difficult to assess the degeneracy between the peak of the second flare, the flux density and the contribution from the emission at lower frequencies. However, higher frequencies reveal smaller spatial scales closer to the base of the jet, indicating that the second flare originated at smaller radii. In addition, changes in the spectral slope moving from optically thin ( $\alpha < 0$ ) to optically thick ( $\alpha > 0$ ) emission at higher frequencies throughout the four epochs indicate increases in either the particle energy density or  $B$  (see Fig. 1a,b).

Contemporaneous X-ray observations also showed increased emission, which we associate with the radio re-brightening. In general, X-ray emission in low-AGN is modelled with a fiducial power law attributed to either the inverse Compton scattering of disk photons<sup>20</sup>, synchrotron<sup>21</sup> or synchrotron self-Compton<sup>15</sup> emission from a jet. In Fig. 2a,b the 2011 absorption-corrected light curves in the 0.5–2 and 2–10 keV X-ray bands are shown. The low-energy band shows strong evidence for a flare at MJD = 55816–55838, whereas the high-energy band does not show such an obvious trend. Owing to the lack of sampling before the start of the initial radio flare, it is unclear if a similar event preceded this flare. However,

<sup>1</sup>Department of Physics, Stanford University, 382 Via Pueblo Mall, Stanford, California 94305, USA. <sup>2</sup>Department of Astronomy, University of Michigan, 1085 S. University Avenue, Ann Arbor, Michigan 48109-1107, USA. <sup>3</sup>Department of Physics and Astronomy, York University, Toronto, M3J 1P3 Ontario, Canada. <sup>4</sup>Hartebeesthoek Radio Observatory, PO Box 443, Krugersdorp 1740, South Africa. <sup>5</sup>National Radio Astronomical Observatory, PO Box O, Socorro, New Mexico 87801, USA. <sup>6</sup>NRC Dominion Radio Astrophysical Observatory, Penticton, British Columbia V2A 6J9, Canada. \*e-mail: [ashking@stanford.edu](mailto:ashking@stanford.edu)

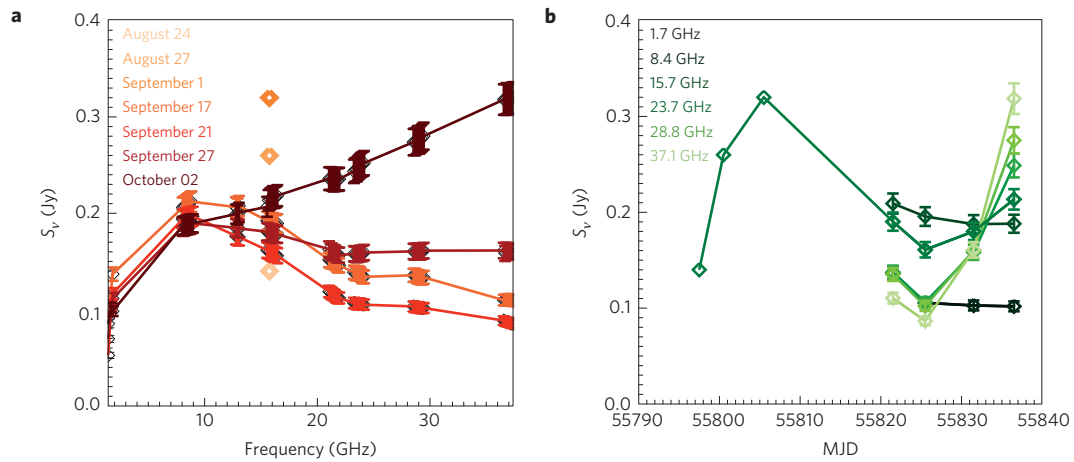


**Figure 1 | Radio flare spectral energy distribution.** Flux density measurements of M81\* at eight radio frequency bands between 1.7–37.1 GHz are shown. Our own observations (filled symbols) were made with the VLA at four epochs from 17 September 2011 (MJD 55821.7) to 2 October 2011 (MJD 55836.7) and we also plot earlier 15 GHz observations (open symbols) made with the Arcminute Microkelvin Imager of the Mullard Radio Astronomy Observatory<sup>18</sup>. **a**, The radio spectral energy distribution at different epochs. Between 17 September and 27 September, the spectrum turns over at  $\sim 10$  GHz, suggesting that it is optically thin above that frequency and that the flare is decaying. However, on 2 October, the whole spectrum is inverted, suggesting that it has become optically thick and that the flare is re-brightening at least at the higher frequencies. **b**, The flux density ( $S_\nu$ ) of different frequencies as a function of MJD. Error bars are the  $1\sigma$  confidence.

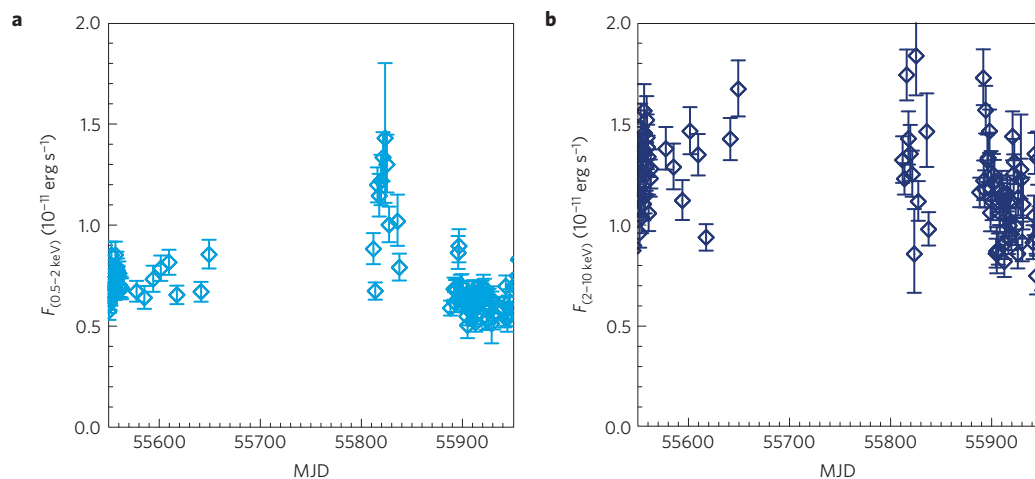


**Figure 2 | X-ray flare.** The X-ray flux ( $F$ ) as a function of time, observed with the Swift satellite. **a**, The absorption-corrected flux in the low-energy, 0.5–2 keV X-ray band. The flux remains relatively constant except for the flare that occurs during MJD = 55816–55838. **b**, The absorption-corrected flux in the high-energy, 2–10 keV X-ray band. There is no obvious flare in this band that can be associated with either the flares in the radio (Fig. 1) or the low-energy X-ray band. Error bars are the  $1\sigma$  confidence.

analysis of all of the archival M81\* Swift data finds this event to be unique in the six years of data (2006–2011), signalling its rare nature (see Supplementary Methods). As M81\* is known to have many radio flares (although with lower intensities) the rare X-ray behaviour associated with this flare may explain its peculiar behaviour, including the first detection of a discrete knot in M81\*, which we discuss in more detail below.

Interestingly, the lack of a strong flare in the high-energy band suggests that the ‘corona’—which is responsible for the production of the high-energy X-rays via inverse comptonization in AGN<sup>20</sup>—is not associated with this particular radio flare. In addition, the X-ray luminosity at 2–10 keV did not vary as dramatically as the emission at low frequencies, which suggests that even during this type of event M81\* would still lie on the fundamental plane of black hole activity. Conversely, the low-energy X-ray emission does seem to be associated with the radio flare at higher frequencies. It precedes the radio re-brightening by at least  $t_{\text{delay}} > 12 \pm 1$  days, determined via a  $Z$ -transformed cross-correlation analysis. We note that the core

is not in a flaring mode nearly three months later on 16 January 2012 based on its flux density and optically thin spectral index, which also sets an upper limit on  $t_{\text{delay}}$  of three months. This last epoch will be discussed below.

Accelerated charged particles in the jet core will cool via synchrotron radiation, and therefore the spectra will peak at progressively lower frequencies at later times. The time lag between the peak emission at different frequencies is dependent on the magnetic field strength, velocity of the flow, and viewing angle<sup>4,5</sup>, as long as adiabatic losses do not dominate<sup>1</sup>. As will be discussed below, we find a one-sided VLBA radio knot moving with an apparent velocity of  $v_{\text{app}}/c = 0.51 \pm 0.17$  and a viewing angle to our line-of-sight of  $\theta < 56^\circ$ . Assuming the de-projected velocity is close to the bulk flow velocity, we constrain  $B$  from the time lag between the X-ray flare and radio re-brightening to be  $1.6 < B < 9.2$  G. We assumed  $\theta = 14^\circ$  (ref. 8) for the upper limit, whereas the minimum flux ratio and maximum  $t_{\text{delay}}$  give the lower limit. This is consistent with the values of  $B$  derived from the peak of the radio

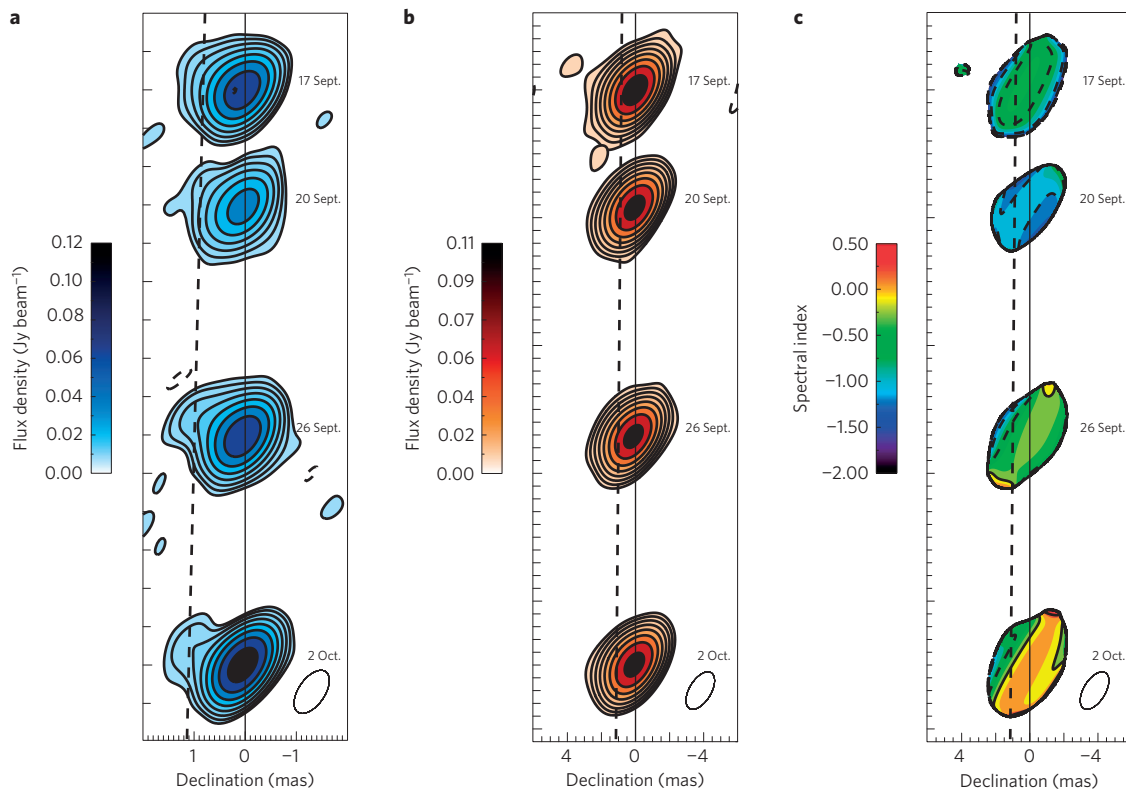


**Figure 3 | High-resolution radio knot motion.** **a–c**, The AGN core and knot emission from M81\* at 23.7 GHz (**a**), 8.4 GHz (**b**) and the resulting spectral index (**c**;  $S_\nu \propto \nu^\alpha$ ) on 17 September (MJD 55821.7), 20 September (MJD 55824.8), 26 September (MJD 55830.8) and 2 October (MJD 55836.7) 2011. The contour levels in **a** are  $3.4 \times (-3, 3, 6, 12, 24, 48, 96, 192, 384) \times 10^{-4}$  Jy beam $^{-1}$  with a restoring beam size of  $1.2 \times 0.55$  mas with a position angle of  $-23.0^\circ$ . The contour levels in **b** are  $2.9 \times (-3, 3, 6, 12, 24, 48, 96, 192, 384) \times 10^{-4}$  Jy beam $^{-1}$  with a restoring beam size of  $3.1 \times 1.4$  mas with a position angle of  $-21.0^\circ$ . And the contours in **c** are  $(-3, -2.5, -2, -1.5, -1, -0.1, 0, 0.5, 1)$  with the negative values shown by dashed lines and a restoring beam size of  $3.1 \times 1.4$  mas with a position angle of  $-21.0^\circ$ . The solid lines denote the position of the core emission. A knot is clearly detected in all four epochs at 23 GHz. Gaussian fits suggest a velocity of  $v_{\text{app}}/c = 0.51 \pm 0.17$ , given by the dashed vertical line. In addition, the core emission moves from a negative index in the first three epochs, to a positive index in the last epoch as it becomes optically thick during the beginning of the second flare. There is a hint that the knot emission has a negative spectral index even during the last epoch, suggesting it is optically thin as it propagates outward. Error bars are the  $1\sigma$  confidence.

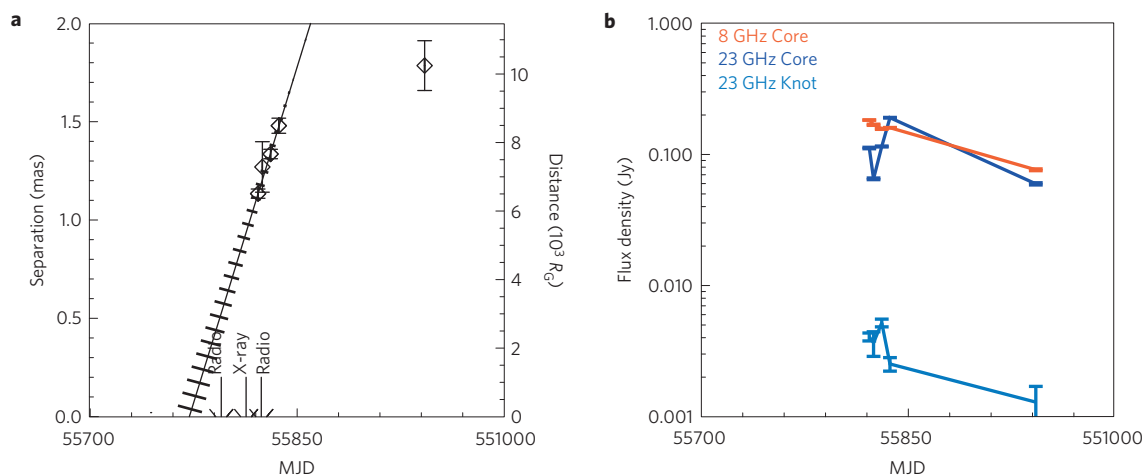


**Figure 4 | Changes in knot position and brightness.** **a**, The relative separation of the knot compared with the centre of the core. The linear fit to the first four epochs (solid line) corresponds to an apparent velocity of  $v_{\text{app}}/c = 0.51 \pm 0.17$ . Owing to the close proximity of M81\* we are able to resolve discrete knot ejections in a compact radio core at high radio frequencies. The fifth data point is possibly associated with the second radio flare or a recollimation shock. **b**, The 23.7 GHz flux density of the knot and core are shown as well as the 8.4 GHz flux density of the core. Error bars are the  $1\sigma$  confidence.

spectral energy distribution in the first epoch,  $B < 10.2$  G (see the Supplementary Methods for further modelling details).

Our measurement of the magnetic field is nearly two orders of magnitude greater than what is measured from the radio core-shift

of M81\*, which results in a value on the order of  $B \sim 34$  mG at 0.21 mas ( $1,300R_G$ ) scales at 8.4 GHz (ref. 12). Even if we extrapolate to 23 GHz, assuming the magnetic field is inversely correlated with radius, we find that  $B$  measured from the core shifts is  $B \sim 90$  mG

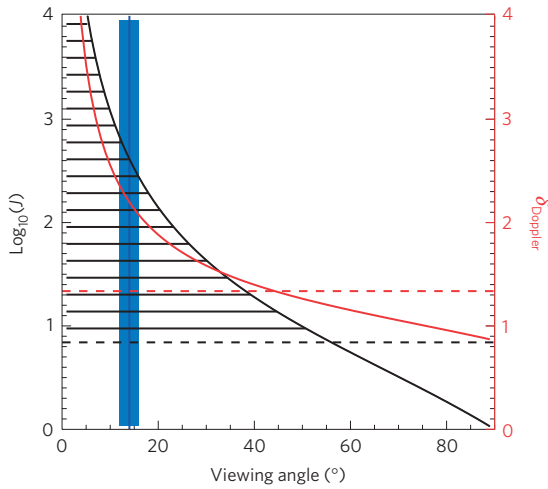


**Figure 5 | Constraints on orientation.** The brightness ratio ( $J$ ) of the approaching and receding knots is shown as a function of viewing angle ( $\theta$ ) in black. The dashed black line shows the lower limit to the ratio of the brightest knot on the third epoch, which puts a limit of the viewing angle of  $\theta < 56^\circ$ . The Doppler factor ( $\delta_{\text{Doppler}}$ ; in red) is shown as a function of  $\theta$ . We measure a Doppler factor from the knot variability during the four epochs (shown as the red dashed line), which corresponds roughly to an inclination of  $\theta \sim 44^\circ$ . The blue vertical line shows the inclination of  $\theta = 14^\circ \pm 2$ , measured from spectral fitting<sup>8</sup>. The errors on the inclination are  $1\sigma$ .

at  $\sim 0.08$  mas ( $\sim 500R_G$ ), which is still two orders of magnitude less than our measurements at much smaller radii. Although this discrepancy could be due to measuring different components of the magnetic field via the two different methods, it is more likely that we are measuring an increase in the magnetic field associated with the large flare event. The magnetic field scales as  $B \propto \nu_p^5 S_p^{-2} \theta_A^4$ , where

$\theta_A$  is the angular size<sup>6</sup>. Even with such a large increase in  $B$ , only a small increase in either the peak frequency or emitting region is required to explain the increase in flux density observed during the flares—both of which are reasonable assumptions, as we note that the peak frequency does in fact increase in the re-brightening of the flare, and the emitting region extends, as evidenced by the detection of the knot discussed below.

We note that the radiation energy density determined via the radio luminosity of the knot is much less than the magnetic energy density determined via synchrotron losses. If the particle energy density is roughly in equipartition with the magnetic field, our results imply that the internal energy of the particles and field dominate over the radiative energy, similar to what is observed in more massive AGN<sup>22</sup> and the stellar-mass black hole Cygnus X-1 (ref. 23).

In addition to having a strong magnetic field, we detect a discrete knot moving at mildly relativistic speeds for the first time in M81\*. Figure 3a shows the knot as it moves radially outward over the four VLBA epochs, taken at 23.7 GHz with a full-width half-maximum (FWHM) restoring beam of  $1.2 \times 0.55$  mas with a position angle of  $-23^\circ$ . Figure 3b shows the 8.4 GHz observations, which have a larger restoring beam of  $3.1 \times 1.4$  mas with a position angle of  $21^\circ$  that makes detection of the knot difficult in all but the last epoch. Figure 3c shows the spectral index,  $\alpha$ , between 8.4 and 23.7 GHz. At a distance of  $3.96 \pm 0.29$  Mpc (ref. 7), 1 mas corresponds to  $4.0 \times 10^3$  AU, or equivalently,  $5.7 \times 10^3 R_G$ , where  $R_G = GM_{\text{BH}}/c^2$  and  $M_{\text{BH}} = 7^{+2}_{-1} \times 10^7 M_\odot$ , which indicates that the knot has a projected distance of  $R_{\text{projected}} \sim 7,500 R_G$ .

The elongation of the nucleus at 8.4 GHz has been observed before<sup>10–12,15,24,25</sup>. However, we are the first to measure the radial motion of the knot in M81\*. Fitting the knot detected at 23.7 GHz with a Gaussian component and determining its position with respect to the brightest component, that is, the core, we find that the knot is moving radially from the centre of the radio core with

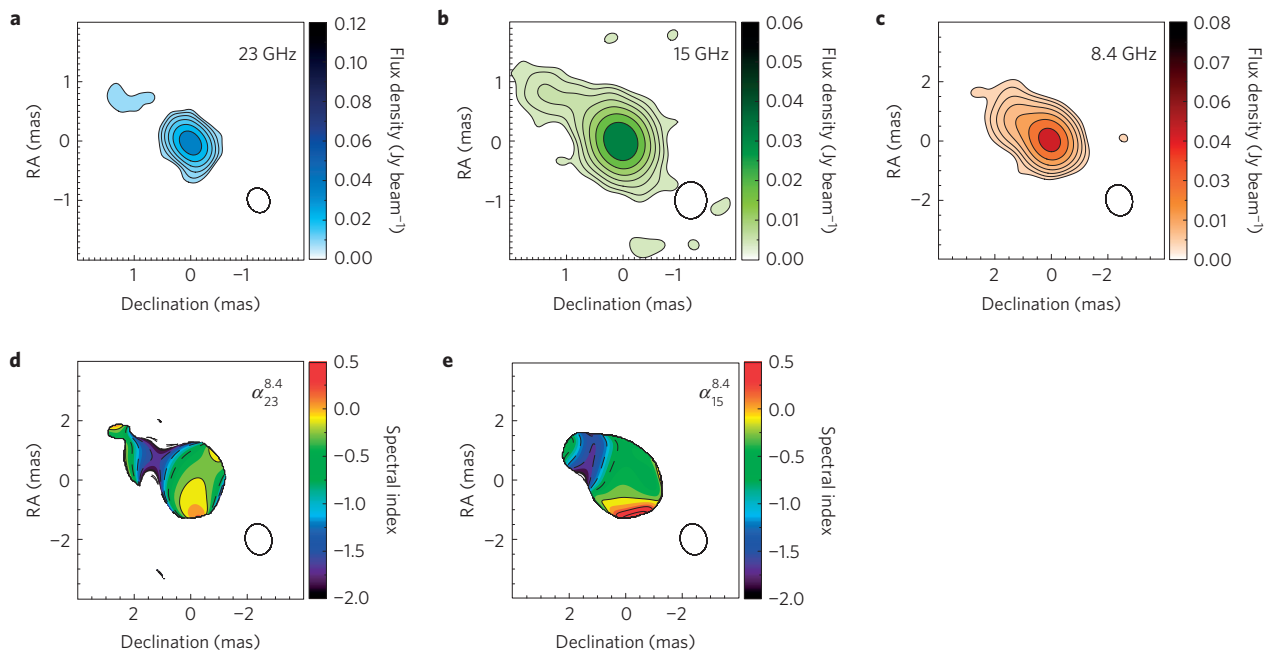


**Figure 6 | VLBA 16 January 2012 (MJD 55943) observations.** **a–e**, The 23.7 GHz (**a**), 15 GHz (**b**), 8.4 GHz (**c**), and spectral index maps of the core between 8.4 and 23 GHz (**d**) and 8.4 and 15 GHz (**e**). In **a–c** the contours are  $\sigma_{\text{rms}} \times (-3, 3, 6, 12, 24, 48, 96, 192, 384) \times 10^{-3}$  Jy beam<sup>-1</sup>, where  $\sigma_{\text{rms}}$  is 0.32, 0.15 and 0.22 mJy beam<sup>-1</sup>, respectively. Panels **d** and **e** have contours of  $(-3, -2.5, -2, -1.5, -1, -0.1, 0, 0.5, 1)$ . The restoring beams are shown in the bottom right corner; **a**,  $0.43 \times 0.38$  mas with a position angle of  $36^\circ$ , **b**  $0.62 \times 0.56$  mas with a position angle of  $-0.6^\circ$ , and **c, d**  $1.1 \times 0.93$  mas with a position angle of  $21^\circ$ . As can be seen in **a–c**, the knot is extended much further from the core than in previous observations. **d** and **e** show that the core and knot are both optically thin ( $\alpha < 0$ ), indicating that the flare has stopped.



a projected velocity of  $v_{\text{app}}/c = 0.51 \pm 0.17$  (see Fig 3a and Fig 4a). Assuming the jet is bipolar, the apparent velocity, together with the lower limit on the brightness ratio from the one-sided detection, place a constraint on the viewing angle of  $\theta < 56^\circ$  to our line of sight. See Fig. 5.

This limit is broadly consistent with the angle of  $\theta = 14^\circ \pm 2$  determined via optical modelling of the accretion disk on parsec scales<sup>8</sup>. However, high-resolution radio studies have found evidence that the core emission in M81\* bends in the plane of the sky on milliarcsec scales<sup>11</sup> and precesses on a timescale of years<sup>11,12,25</sup>, which suggests that the inclination may change even on small scales and long time periods. Longer observations during similar outburst events are needed to further constrain the inclination angle.

As the knot moves radially outward, its brightness also changes. Figure 4b shows the variability observed in both the knot and core at 23.7 GHz, as well as the variability observed in the core at 8.4 GHz. The core emission becomes optically thick by the end of the four epochs, which can also be seen in the spectral index map in Fig. 3c. Figure 3c suggests that the knot is optically thin throughout the four epochs. The knot does however continue to brighten until the third epoch, and then drops in flux density by the fourth epoch. See Fig. 4b. The variability of the knot as it moves out along the jet can be used to estimate the Doppler factor<sup>1</sup>,  $\delta_{\text{Doppler}}$ , shown by the red curve in Fig. 5. We discuss this in more detail in the Supplementary Methods, and find the Doppler factor to be  $\delta_{\text{Doppler}} \sim 1.5$ . This corresponds to a viewing angle of  $\theta \sim 44^\circ$ , which is much larger than the angle inferred from optical modelling. However, large uncertainties due to the poor temporal sampling of the knot light curve do not exclude a  $\theta = 14^\circ$ .

We also reduced archival VLBA observations of M81\* on 16 January 2012 (MJD 55943), nearly three months later, which also show a discrete knot in addition to the compact core emission at both 23 GHz and 15 GHz (Fig. 6a–e). Again, due to the lack of temporal sampling, we can not distinguish between a separate, distinct knot ejection associated with the re-brightening of the core, stalling of the original knot or a recollimation of the jet. The January knot might have been launched during the radio re-brightening flare if the velocity is less than that observed for the first knot. In contrast, the knot may have decelerated to the position in this fifth epoch. The recollimation of jets and deceleration of knots is observed for other jets, such as M87 (ref. 2), but at much larger gravitational radii ( $\sim 10^6 R_G$ ) compared with what is observed for M81\*.

The closeness of the bright knots to the core in M81\*,  $R < 10^5 R_G$  (for all but the smallest inclinations,  $\theta \lesssim 6^\circ$ ) is peculiar when compared with other AGN that have similar masses but are radio loud, for example, 3C 120 and 3C 111 (refs 26,27). These latter AGN produce jets that reach radial extents exceeding  $R > 10^6 R_G$ . The mildly relativistic knot velocity may partially explain the small radial extent of M81\*, as the knot may not travel as far before dissipating. However, this can not be the only solution, as M87 has both mildly relativistic knots at small radii and highly relativistic knots at large radii<sup>2</sup>. Therefore, a high magnetic field strength, a high accretion rate, small black hole mass or even a potentially low spin may be responsible for setting the small radial extent in M81\*.

Current paradigms suggest that jet production in both stellar-mass and supermassive black holes with low mass accretion rates should be steady and continuous<sup>3</sup>, whereas black holes with high mass accretion rates,  $L_X \sim L_{\text{Edd}}$ , produce jets with discrete, highly relativistic knots<sup>26–28</sup>. As M81\* has a relatively low-mass supermassive black hole ( $7 \times 10^7 M_\odot$ ; ref. 8) and is accreting material at a very low rate ( $L_X \sim 10^{-5.8} L_{\text{Edd}}$ ), the detection of discrete, mildly relativistic knots reveals the similarities between jet production at all masses and mass accretion rates. The observations demonstrate that although the radial extent and knot velocities may differ, jets are intrinsically capable of producing the same knot-like structures. In addition, the multiwavelength analysis indicates that jet knot

ejections are not only associated with radio flares, but also X-ray flares, and can be used to measure the magnetic field strength very close to the black hole.

Received 5 January 2015; accepted 9 March 2016;  
published online 18 April 2016

## References

- Jorstad, S. G. *et al.* Polarimetric observations of 15 active galactic nuclei at high frequencies: jet kinematics from bimonthly monitoring with the very long baseline array. *Astron. J.* **130**, 1418–1465 (2005).
- Asada, K., Nakamura, M., Doi, A., Nagai, H. & Inoue, M. Discovery of sub- to superluminal motions in the M87 jet: an implication of acceleration from sub-relativistic to relativistic speeds. *Astrophys. J.* **781**, L2 (2014).
- Falcke, H., Kording, E. & Nagar, N. M. Compact radio cores: from the first black holes to the last. *New Astron. Rev.* **48**, 1157–1171 (2004).
- Urry, C. M. *et al.* Multiwavelength monitoring of the bl lacertae object PKS 2155–304 in 1994 May. III. Probing the inner jet through multiwavelength correlations. *Astrophys. J.* **486**, 799–809 (1997).
- Bai, J. M. & Lee, M. G. Radio/X-ray offsets of large-scale jets caused by synchrotron time lags. *Astrophys. J.* **585**, L113–L116 (2003).
- Kellermann, K. I. & Pauliny-Toth, I. I. K. Compact radio sources. *Annu. Rev. Astron. Astrophys.* **19**, 373–410 (1981).
- Bartel, N., Bietenholz, M. F., Rupen, M. P. & Dwarkadas, V. V. SN 1993J VLBI. IV. A geometric distance to M81 with the expanding shock front method. *Astrophys. J.* **668**, 924–940 (2007).
- Devereux, N., Ford, H., Tsvetanov, Z. & Jacoby, G. STIS spectroscopy of the central 10 parsecs of M81: evidence for a massive black hole. *Astron. J.* **125**, 1226–1235 (2003).
- de Bruyn, A. G., Crane, P. C., Price, R. M. & Carlson, J. B. The radio sources in the nuclei of NGC 3031 and NGC 4594. *Astron. Astrophys.* **46**, 243–251 (1976).
- Bartel, N. *et al.* The nucleus of M81—simultaneous 2.3 and 8.3 GHz mark III VLBI observations. *Astrophys. J.* **262**, 556–563 (1982).
- Bietenholz, M. F., Bartel, N. & Rupen, M. P. The location of the core in M81. *Astrophys. J.* **615**, 173–180 (2004).
- Martí-Vidal, I. *et al.* Detection of jet precession in the active nucleus of M81. *Astron. Astrophys.* **533**, A111 (2011).
- Ishisaki, Y. *et al.* X-ray properties of the nucleus of M81. *Publ. Astron. Soc. Jpn* **48**, 237–248 (1996).
- Merloni, A., Heinz, S. & di Matteo, T. A fundamental plane of black hole activity. *Mon. Not. R. Astron. Soc.* **345**, 1057–1076 (2003).
- Markoff, S. *et al.* Results from an extensive simultaneous broadband campaign on the underluminous active nucleus M81\*: further evidence for mass-scaling accretion in black holes. *Astrophys. J.* **681**, 905–924 (2008).
- Miller, J. M., Nowak, M., Markoff, S., Rupen, M. P. & Maitra, D. Exploring accretion and disk-jet connections in the LLAGN M81\*. *Astrophys. J.* **720**, 1033–1037 (2010).
- Ho, L. C., van Dyk, S. D., Pooley, G. G., Sramek, R. A. & Weiler, K. W. Discovery of radio outbursts in the active nucleus of M81. *Astron. J.* **118**, 843–852 (1999).
- Pooley, G. Radio flare in M81. *Astron. Telegr.* **3621**, 1 (2011).
- Cotton, W. D. *et al.* The very flat radio spectrum of 0735 plus 178—a cosmic conspiracy. *Astrophys. J.* **238**, L123–L128 (1980).
- Merloni, A. & Fabian, A. C. Coronal outflow dominated accretion discs: a new possibility for low-luminosity black holes? *Mon. Not. R. Astron. Soc.* **332**, 165–175 (2002).
- Markoff, S., Nowak, M. A. & Wilms, J. Going with the flow: can the base of jets subsume the role of compact accretion disk coronae? *Astrophys. J.* **635**, 1203–1216 (2005).
- Merloni, A. & Heinz, S. Measuring the kinetic power of active galactic nuclei in the radio mode. *Mon. Not. R. Astron. Soc.* **381**, 589–601 (2007).
- Gallo, E. *et al.* A dark jet dominates the power output of the stellar black hole cygnus X-1. *Nature* **436**, 819–821 (2005).
- Bietenholz, M. F. *et al.* VLBI observations of the ultracompact radio nucleus of the galaxy M81. *Astrophys. J.* **457**, 604–609 (1996).
- Bietenholz, M. F., Bartel, N. & Rupen, M. P. A stationary core with a one-sided jet in the center of M81. *Astrophys. J.* **532**, 895–908 (2000).
- Chatterjee, R. *et al.* Disk-jet connection in the radio galaxy 3C 120. *Astrophys. J.* **704**, 1689–1703 (2009).
- Chatterjee, R. *et al.* Connection between the accretion disk and jet in the radio galaxy 3C 111. *Astrophys. J.* **734**, 43–59 (2011).
- Wehrle, A. E. *et al.* Kinematics of the parsec-scale relativistic jet in quasar 3C 279: 1991–1997. *Astrophys. J. Suppl.* **133**, 297–320 (2001).

## Acknowledgements

A.L.K. acknowledges support provided by NASA through an Einstein Postdoctoral Fellowship (grant number PF4-150125) awarded by the Chandra X-ray Center, which is

operated by the Smithsonian Astrophysical Observatory for NASA under contract NAS8-03060.

### Author contributions

A.L.K. led the data reduction and analysis, with contributions from J.M.M., M.B. and A.M. K.G., M.T.R., M.R. and N.B. contributed to discussion and interpretation.

### Additional information

Supplementary information is available in the [online version of the paper](#). Reprints and permissions information is available online at [www.nature.com/reprints](http://www.nature.com/reprints). Correspondence and requests for materials should be addressed to A.L.K.

### Competing financial interests

The authors declare no competing financial interests.